JAWRA Journal of the American Water Resources Association

AMERICAN WATER RESOURCES ASSOCIATION

RESEARCH ARTICLE

Assessing Climate Change Vulnerability of Hydropower Production and Water Supply in the Mediterranean Hotspot

Emrah Yalcin | Cansu Boz

Department of Civil Engineering, Kirsehir Ahi Evran University, Kirsehir, Turkey

Correspondence: Emrah Yalcin (emrah.yalcin@ahievran.edu.tr)

Received: 24 July 2025 | **Revised:** 11 November 2025 | **Accepted:** 16 January 2026

Keywords: climate change | hydropower | multi-model ensemble | reservoir operation | SWAT model | water supply

ABSTRACT

Appraising the possible impacts of a changing climate on water resources infrastructure is essential for ensuring long-term sustainability, particularly in vulnerable regions such as the Mediterranean hotspot. This study applies an integrated modeling framework to evaluate the operational reliability of the Karakuz Dam and Hydroelectric Power Plant, a multi-purpose project located in southern Turkey. The framework utilizes daily bias-corrected precipitation and temperature data from 24 Global Circulation Models (GCMs) that are part of the Coupled Model Intercomparison Project Phase 6 (CMIP6). The best-performing GCMs are combined into multi-model ensembles under two shared socio-economic pathways (SSPs), SSP2-4.5 and SSP5-8.5, along with the CMIP6 historical experiment. Reservoir inflows are modeled using the Soil and Water Assessment Tool (SWAT), while lake evaporation estimates are included to determine the total available water volume for hydropower generation, domestic use, and downstream ecological flow requirements. Results indicate potential reductions in hydropower production of up to 16.6% under SSP2-4.5 and up to 46.6% under SSP5-8.5. Despite these reductions, designated domestic and environmental demands are projected to be met under both future scenarios. The study highlights the critical importance of adaptive water management strategies to mitigate adverse climate impacts and preserve the resilience and functionality of hydropower systems.

1 | Introduction

The Mediterranean region (10°W to 40°E, 30°N to 45°N) is widely recognized as a prominent hotspot, experiencing the impacts of global warming more acutely than many other regions (Giorgi 2006; Iturbide et al. 2020) (Figure 1). Encompassing countries such as Algeria, Bulgaria, Cyprus, Egypt, Greece, Jordan, Lebanon, Libya, Malta, Morocco, Portugal, Spain, Syria, Tunisia, and Turkey, the region and its sub-regions are consistently projected to experience ongoing atmospheric and oceanic warming, substantial increases in temperature, and significant changes in precipitation patterns (Cherif et al. 2020; Ali et al. 2022). These projections have raised growing concerns about reductions in the ability of reservoirs to retain water, primarily due to the joint influence of anticipated changes in rainfall and temperature regimes affecting critical aspects of water cycle dynamics, including river flows, water requirements, and lake evaporative losses (Masia et al. 2018; Tramblay et al. 2020). Nonetheless, simulating climate-induced hydrological changes in the Mediterranean region presents considerable challenges due to the region's complex topography and pronounced spatial and temporal climate variability (Michaelides et al. 2018). Hence, the use of high-quality climate data is essential for adequately assessing regional- and local-scale impacts (Zittis et al. 2022).

Global Circulation Models (GCMs) simulate future climate conditions by incorporating physical processes and interactions within and between various elements of the climate system, such as the atmosphere, biosphere, cryosphere, hydrosphere, and terrestrial surface (Cos et al. 2022). The Coupled Model Intercomparison Project (CMIP), which organizes the development and dissemination of GCM simulations for historical,

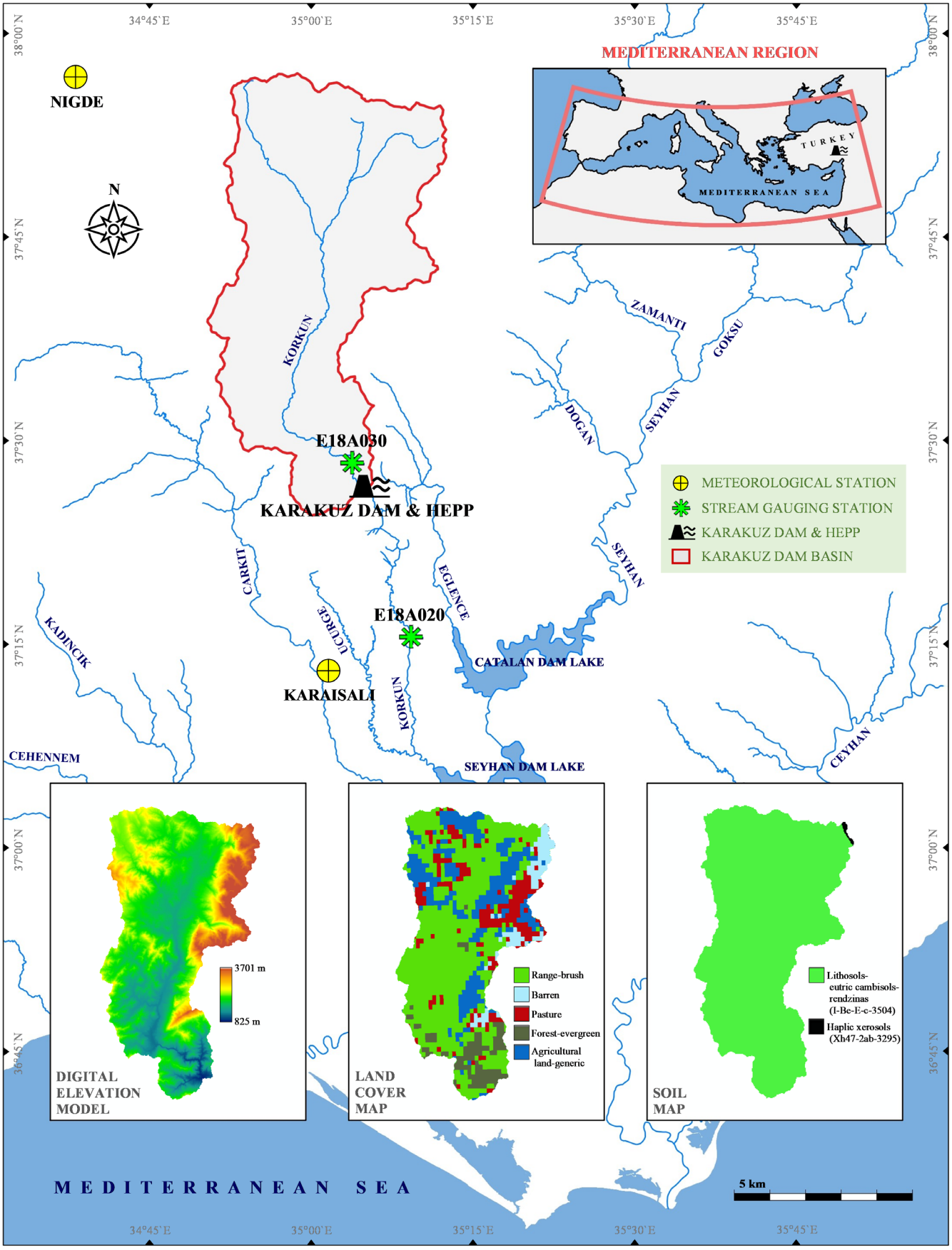

FIGURE 1 | Location map of the Karakuz Dam basin, including key geospatial characteristics.

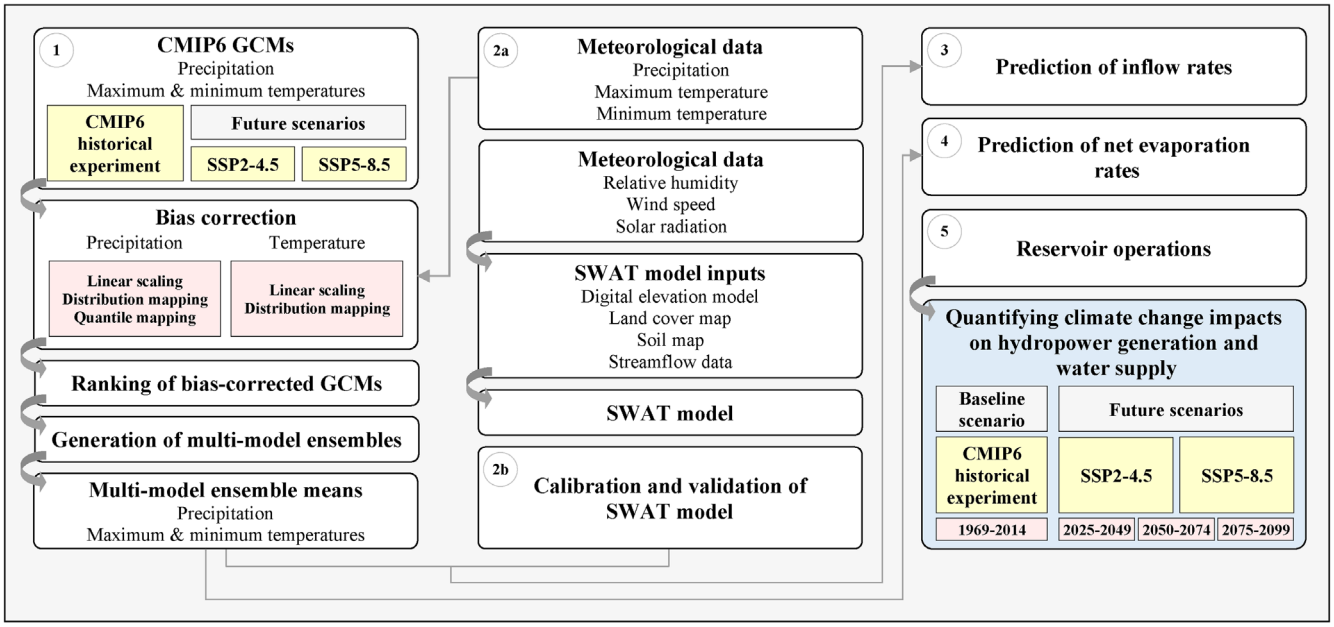

FIGURE 2 | Schematic representation of the methodology employed in this study.

current, and future climates, has become a cornerstone of climate science by providing a wide range of model outputs to enhance understanding of climate variability and change (Eyring et al. 2016). The most recent sixth phase, CMIP6, places greater emphasis on radiative forcing driven by both anthropogenic and natural influences (Stouffer et al. 2017). CMIP6 projections rely on shared socio-economic pathways (SSPs), which designate future emissions and land utilization trajectories under alternative societal development scenarios (O'Neill et al. 2016). For example, SSP2-4.5 assumes moderate implementation of climate policy and simulates a radiative forcing of 4.5 W/m^2 by century's end, while SSP5-8.5 characterizes a high-emissions scenario, reaching 8.5 W/m^2 (Riahi et al. 2017).

Although CMIP6 projections are broadly consistent with those from previous phases (CMIP3 and CMIP5), some CMIP6 models simulate significantly higher warming magnitudes (Tokarska et al. 2020). Cos et al. (2022) compared multiple CMIP5 and CMIP6 model simulations to assess evolving climate impacts in the Mediterranean region. Their findings suggest that, by century's end, summer temperatures may rise by 1.83°C–8.49°C under CMIP6 and by 1.22°C–6.63°C under CMIP5. Additionally, summer precipitation is projected to decrease by 16%–49% under CMIP6 and by 22%–47% under CMIP5. Focusing on Turkey, Bağçaci et al. (2021) analyzed the historical simulations of CMIP5 and CMIP6 models in terms of precipitation and temperature, and quantified potential future changes under different SSP scenarios using ensemble means from the best-performing models. Their analysis showed that CMIP6 models provided clearer precipitation trends and higher spatial resolution than CMIP5. In addition, CMIP6 projections suggest that summer temperatures across the country could rise by up to 6.5°C, and autumn precipitation could decline by up to 40%. While several other assessments have explored how the future may influence the hydro-climatic conditions of Mediterranean catchments using CMIP6 projections, research examining how these changes may affect reservoir operational efficiency and long-term sustainability remains limited (Yalcin 2024). Quantifying the potential hydrological impacts of a changing climate through scenario-based numerical modeling is essential for minimizing risks through appropriate design and operation of reservoir systems (Jiménez-Navarro et al. 2021).

In this context, the present study investigates the potential influence of forthcoming climate variability and change on the intended hydropower and water supply functions of the Karakuz Dam and Hydroelectric Power Plant (HEPP), located in the Seyhan River basin in southern Turkey (Figure 1). The Karakuz Project, commissioned in 2015, was dimensioned using historical hydro-meteorological observations to utilize a 573 m head for hydropower production and to partially meet the future water needs of Nevsehir province (Dolsar 2008; Alarko 2023). The study employs a methodological framework encompassing five principal steps: (1) generation of daily precipitation and temperature projections under the multi-model ensemble (MME) approach for the CMIP6 historical experiment and the future pathway scenarios of SSP2-4.5 and SSP5-8.5; (2) construction of a Soil and Water Assessment Tool (SWAT) model for the Karakuz Dam watershed and its calibration; (3) simulation of monthly mean inflows to the Karakuz Dam using the calibrated model and climate projections; (4) calculation of mean monthly net lake evaporation rates based on climate projections; and (5) simulation of reservoir operations using a monthly operational algorithm informed by projected inflows and evaporation estimates. The possible short-, mid-, and long-term impacts of hydro-climatic change on hydropower generation and water supply are assessed under the considered pathway scenarios for the periods 2025–2049, 2050–2074, and 2075–2099. This framework is schematically illustrated in Figure 2. This study is principally intended to emphasize the need to implement adaptive strategies in the planning and operation of reservoir systems in response to evolving climate conditions, particularly given the growing water scarcity risks for the riparian countries of the Mediterranean.

2 | Study Area and Hydro-Climatological Data

2.1 | Karakuz Dam and HEPP Project

The study area is situated within the Seyhan River basin, which spans both the Mediterranean and Central Anatolian regions of Turkey (Figure 1). Covering a drainage area of 22,035 km^2, the Seyhan basin is between the latitudes 36°30′ and 39°15′N, and the longitudes 34°45′ and 37°00′E (SYGM 2020). The principal tributaries of the Seyhan River include the Goksu, Zamanti, and Korkun creeks. Korkun Creek flows within the administrative boundaries of the Pozanti and Karaisali districts of Adana province. Originating at an elevation of approximately 2200 m under the name Ecemis Brook, it is later referred to as Kamisli Brook at around 1250 m and eventually merges with Ucurge Brook at approximately 100 m before discharging into the Seyhan Dam reservoir. The Karakuz Dam and HEPP is the only dam project on Korkun Creek (Figure 1). The Karakuz Dam has a drainage area of 1261.47 km^2. As the dam basin encompasses parts of the Taurus Mountain Range in southern Turkey (i.e., Bolkar and Aladaglar), the basin is predominantly characterized by mountainous and rugged topography and is underlain geologically by mesozoic peridotites (Dolsar 2008; Alarko 2023).

The Karakuz Dam and HEPP Project was designed to utilize a hydraulic head of 573 m, spanning elevations from 831 to 258 m along Korkun Creek. Constructed at a thalweg elevation of 800 m, the dam has a structural height of 32.5 m. The reservoir's maximum and minimum water levels are 831 and 818 m, respectively. At maximum reservoir level, the storage volume is 5112 hm^3; at minimum level, it is 1695 hm^3, providing an active storage capacity of 3417 hm^3. The stored water is diverted into a 12,476-m-long conveyance system via an intake structure located at a base elevation of 813.5 m, with a design capacity of 16.41 m^3/s. It is then transported through a 1541-m-long, 2-m-diameter penstock to the Karakuz HEPP. The diverted water, reaching the turbine axis at an elevation of 260.2 m, drives two equally rated Pelton-type turbines with a total installed capacity of 76 MW. The tailwater elevation of the HEPP is 258 m. A minimum ecological flow of 0.1 m^3/s is required between the dam and the plant to sustain the ecological integrity of Korkun Creek and its associated habitats, including fish, algae, and other aquatic species, as well as riparian flora and fauna in the downstream reach. In addition, future plans include the withdrawal of 0.4 m^3/s from the Karakuz reservoir to partially meet the domestic water demand of Nevsehir province (Dolsar 2008; Alarko 2023).

2.2 | Meteorological Data

In the scope of this study, daily time series data on precipitation, maximum/minimum temperatures, relative humidity, wind speed, and solar radiation intensity from synoptic meteorological stations (MSs) are required for the development of a hydrological model for the Karakuz Dam basin. Among several MSs in proximity to the basin (e.g., Adana, Aladag, Camardi, Karaisali, Nigde, Pozanti, and Yahyali), the Nigde (ID: 17250) and Karaisali (ID: 17936) stations are identified as having the most temporally extensive and least interrupted datasets (Figure 1) (MGM 2023a, 2023b). The Nigde MS, situated at an elevation of 1211 m, records an average annual total precipitation of 338.3 mm, average annual maximum/minimum temperatures of 17.6°C/5.2°C, an average annual relative humidity of 57.9%, and a mean annual snow depth of 4.3 cm (MGM 2023c). The Karaisali MS, located at an elevation of 240 m, reports an average annual total precipitation of 878.3 mm, average annual maximum/minimum temperatures of 24.3°C/14.0°C, an average annual relative humidity of 59.6%, and a mean annual snow depth of 3.5 cm (MGM 2023d).

2.3 | Streamflow Data

On Korkun Creek, there are two stream gauging stations (SGSs) (Figure 1). The first station, designated E18A020, is the Hacili Bridge SGS, located at an elevation of 167 m and covering a catchment area of 1440.8 km^2. Based on measurements recorded between 1969 and 2014, this station has an average flow rate of 12.56 m^3/s (DSI 2023). The second station, designated E18A030, is the Karakuz SGS, situated at an elevation of 830 m, with a catchment area of 1230.5 km^2. According to data collected between 1996 and 2014, the average flow rate at this station is 6.60 m^3/s (DSI 2023). For the calibration of a hydrological model intended to simulate monthly streamflow rates at the dam site, measurements from the Karakuz SGS are preferred due to its proximity to the dam axis. However, the relatively short observation period of the Karakuz SGS necessitates the extension of its monthly average flow data to cover the period from 1969 to 2014. This extension is based on the strong correlation ($R^2 = 0.96$) between the monthly average flows recorded at the Karakuz and Hacili Bridge SGSs (Figure S1a). The extended monthly flow values at the Karakuz SGS are then transposed to the dam axis utilizing the drainage area ratio between the Karakuz SGS and the Karakuz Dam (Figure S1b). Consequently, the average streamflow rate of Korkun Creek at the Karakuz Dam location is estimated to be 7.93 m^3/s between 1969 and 2014.

2.4 | GCM Data From CMIP6

The World Climate Research Program (WCRP) is a globally prominent institution that has conducted research on the intricate dynamics of the climate system for over four decades. Since 1995, WCRP has coordinated successive phases of CMIP, each designed to enhance scientific understanding of past, present, and projected future climate variability and change. This study utilizes daily precipitation and maximum/minimum temperature outputs simulated by 24 GCMs from the most recent phase of the initiative, CMIP6. These datasets cover both the CMIP6 historical experiment and two future societal development scenarios of SSP2-4.5 and SSP5-8.5 (ESGF 2022). A detailed summary of the model identifiers, institutions, and horizontal resolutions of the considered GCMs is given in Table S1. As several CMIP6 models include multiple ensemble simulations, only the first ensemble member (i.e., r1i1p1f1) is selected to ensure uniformity and facilitate inter-model comparability (Sun et al. 2022). The original GCM outputs, provided in NetCDF format and across varying native spatial grids, are resampled to a uniform resolution of 0.5° × 0.5° over the domain of Turkey. This spatial harmonization is carried out under the first-order conservative

remapping approach proposed by Jones (1999). Preprocessing procedures, including merging, interpolation, and spatial cropping, are performed using the Climate Data Operators (CDO) program (Schulzweida 2021) within the Cygwin terminal environment (Cygwin 2022).

3 | Methods

3.1 | Generating Climate Change Scenarios Using MMEs From CMIP6 GCMs

Raw GCM simulations corresponding to the coordinates of the Nigde and Karaisali stations are extracted from the resampled NetCDF-format projection datasets. These datasets include daily historical precipitation and temperature data for the 1965–2014 period, along with future pathway projections for 2020–2099. All data are subjected to bias correction to minimize potential systematic errors. For raw precipitation data, bias correction is applied using three different statistical downscaling methods, while two methods are used for temperature data. Specifically, linear scaling (LS), distribution mapping (DM), and quantile mapping (QM) are applied to precipitation, whereas only LS and DM are used for temperature. The LS and DM methods are applied using the CMhyd software (Rathjens et al. 2016), while QM is implemented using the Qmap package in the R environment (Gudmundsson 2022). Observational data from the stations during 1965–2014 are used as the reference for the bias correction procedures.

The simulation performance of each GCM with each bias correction method is independently evaluated by comparing historical simulations against measurements at the Nigde and Karaisali MSs. In the first stage of evaluation, the performance of each GCM's bias-adjusted monthly mean simulations is assessed using four statistical metrics: modified index of agreement (MD) (Legates and McCabe 1999), normalized root mean square error (nRMSE) (Almeida et al. 2015), Kling-Gupta efficiency (KGE) (Gupta et al. 2009), and fractions skill score (FSS) (Roberts and Lean 2008). Optimal performance is characterized by values approaching 1 for MD, KGE, and FSS, while values approaching 0 are preferred for nRMSE. In the second stage, basin-scale statistics are calculated by weighting station-level metrics by areal coverage. In the final stage, rating metrics (RMs) (Chen et al. 2011) are calculated to consolidate the rankings derived from the four performance metrics for each variable. The best simulation performance in terms of RM is represented by values closest to 1. For precipitation, basin-level RMs determine the best-performing GCMs, while RM rankings for maximum and minimum temperatures are combined to produce a unified GCM ranking.

The literature suggests that using a single GCM, even one with the highest performance, is insufficient to address the uncertainties inherent in climate projections (Wang et al. 2020). MME projections composed of the top-performing 3–10 GCMs have been shown to substantially reduce GCM-related uncertainty (Ahmed et al. 2019). Accordingly, in this study, after ranking the GCMs for each climate variable and bias correction method at the basin scale, the four top-ranked models are considered as ensemble members (Bağçaci et al. 2021). Historical and future daily time series projections from these MMEs are generated for each station by computing the arithmetic mean of the bias-adjusted projections of the member GCMs (Ahmed et al. 2019). Finally, basin-level performance statistics in terms of the MD, KGE, FSS, and nRMSE metrics for the ensembles constructed under different bias correction methods are compared to identify the most effective bias correction method and, hence, the best-performing MME for each climate variable.

3.2 | Modeling Watershed Hydrology Using SWAT

3.2.1 | SWAT Model

SWAT is a semi-distributed model intended to simulate hydrologic processes such as streamflow, water quality, and sediment movement in watersheds of various scales and characteristics over extended periods (Neitsch et al. 2011). In this research, the SWAT model is implemented using ArcSWAT (revision 664) to simulate monthly streamflow in the Karakuz Dam basin. This setup requires the integration of both station-based weather data and spatially distributed watershed data, including topography, land use/cover, and soil characteristics.

The digital elevation model of the Karakuz basin is attained from the Shuttle Radar Topography Mission archive (USGS 2014). The 1 arc-second resolution data indicate elevation values within the basin ranging from 825 to 3701 m (Figure 1). Land cover data are obtained from the Global Land Cover 2000 dataset (EC-JRC 2006). Five distinct land cover classifications are identified within the basin at 1 km spatial resolution: range-brush, barren, pasture, forest-evergreen, and agricultural land-generic (Figure 1). Soil properties are taken from the Digital Soil Map of the World (FAO 2007). Two main soil types are identified from the 1:5 million scale dataset: a composite unit of lithosols-eutric cambisols-rendzinas and haplic xerosols (Figure 1).

Following watershed delineation, the basin is categorized into five slope classes: 0%–5%, 5%–15%, 15%–25%, 25%–50%, and > 50%. In SWAT, hydrologic response units (HRUs) represent the smallest computational elements where hydrological processes are simulated. To eliminate negligible HRU formations, threshold rates of 15%, 5%, and 5% are applied for slope, land use, and soil, respectively, during HRU definition. Accordingly, the model delineates 109 subbasins and produces a total of 733 HRUs for the Karakuz Dam basin.

Observational data from the Nigde MS begin in 1950, while data from the Karaisali MS are available from 1964 onward. Based on the calculated monthly mean streamflow at the dam site for the 1969–2014 period, the model simulation period is set from 1965 to 2014, with the first 4 years (1965–1968) used for model warm-up. To address gaps in the station records, monthly meteorological statistics are also incorporated into the model. Missing dew point temperature values are computed using the dew02 program (Liersch 2003), based on daily maximum/minimum temperatures and relative humidity records. Similarly, missing monthly maximum 30-min rainfall intensities are estimated by multiplying the highest daily rainfall amounts by the station-specific 30-min pluviograph coefficient for each month. Based on station metadata, SWAT allocates weather inputs from the

Nigde and Karaisali MSs to 86 and 23 subbasins, respectively, covering approximately 75% and 25% of the basin.

The final step in the model setup involves delineating elevation bands for each subbasin to consider orographic influences on climate variables (Arnold et al. 2013). The Make_ELEV_BAND utility (Abbaspour 2015) is used to create five elevation bands per subbasin, excluding those with limited elevation variation that would not significantly affect precipitation or temperature gradients.

3.2.2 | Model Calibration

The established model is calibrated using the computed flow rates of Korkun Creek at the Karakuz Dam site for the years 1969–1998 and verified for the years 1999–2014. The calibration process is conducted under the Sequential Uncertainty Fitting Version 2 (SUFI-2) methodology (Abbaspour et al. 2004) within the SWAT Calibration and Uncertainty Procedures (SWAT-CUP) software (Abbaspour 2015). Parameter ranges are used to represent potential uncertainties (i.e., inputs, parameters, and the conceptual model) in the SUFI-2 algorithm, and simulation uncertainty is evaluated considering the 95% prediction uncertainty (95PPU), along with the P-factor and R-factor indices (Abbaspour et al. 2007). In this research, the objective function of SUFI-2 is the Nash-Sutcliffe Efficiency (NSE) (Nash and Sutcliffe 1970). Additionally, in both calibration and validation, the ratio of the RMSE to the standard deviation of the actual data (RSR) and percent bias (PBIAS) statistics is utilized for performance assessment.

The SUFI-2 algorithm is applied in three consecutive steps to mitigate the issue of parameter interaction (Yalcin 2019). In the first step, the parameters related to lapse rate are calibrated and adjusted to the best-performing values. The second step involves the calibration of sensitive basin parameters related to snow, using the same approach as in the first step. The procedure concludes with the calibration of other sensitive parameters (i.e., groundwater, soil, HRU, management, and main channel). At each stage, parameter sensitivity is assessed through single-parameter runs comprising 50 simulations. Subsequently, a combined parameter run of 500 simulations is conducted using the sensitive parameters and their beginning parameter intervals determined during the single runs. This iterative process continues until satisfactory values are achieved for the P-factor, R-factor, and NSE (Abbaspour et al. 2015). The final parameter intervals obtained from the last combined run are considered the calibrated ranges. The parameter set associated with the simulation yielding the highest NSE value (i.e., best simulation) is identified as the best-performing set. Validation is conducted using a single combined run within the calibrated ranges, along with a single simulation using the best-performing set.

3.3 | Streamflow Regime Under Climate Change Scenarios

Using the developed SWAT model with the best-performing parameter rates, three separate simulations are conducted to estimate the monthly average runoff rates of Korkun Creek at the Karakuz Dam site. These simulations incorporate daily climate projections from the best-performing MMEs for the Nigde and Karaisali station locations, based on the CMIP6 historical experiment as well as the SSP2-4.5 and SSP5-8.5 pathway scenarios. For the CMIP6 historical experiment, daily climate projections for the period 1965–2014 are used as historical climate data. The SWAT simulation reproduces monthly inflows to the Karakuz reservoir for the 1969–2014 period, with a four-year model warm-up from 1965 to 1968. Similarly, daily climate projections for the 2021–2099 period are used to estimate monthly average inflows to the reservoir for the years 2025–2099 under the considered pathway scenarios. The impacts of climate change on streamflow regime are assessed using the monthly inflows simulated under the historical experiment as the reference case. Inflow projections under the SSP scenarios are analyzed based on seasonal and annual averages across the near- (2025–2049), mid- (2050–2074), and end-century (2075–2099) periods.

3.4 | Lake Evaporation Under Climate Change Scenarios

Monthly projections of net evaporation from the Karakuz reservoir are derived using a methodology based on the historical relationship between average monthly temperature and total evaporation statistics from the Karaisali station (MGM 2023d) (Figure S1c). To ensure consistency between evaporation values derived from the best-performing MME projections and those from station records, mean temperature is computed as the mean of daily maximum and minimum temperatures (Usul 2009). Assuming a temperature lapse rate of 1°C per 200 m of elevation gain, the average monthly temperatures recorded at the Karaisali MS from 1969 to 2014 are adjusted to account for the elevation corresponding to the reservoir's maximum water level. Based on the established temperature-evaporation relationship at the Karaisali station, the corresponding monthly total evaporation values are estimated using these adjusted temperatures. The resulting evaporation estimates are then converted to actual reservoir evaporation by applying a pan factor of 0.7, in accordance with Usul (2009). Net monthly evaporation amounts per unit reservoir area are obtained by subtracting the average monthly total rainfall rates (1969–2014) from the computed actual evaporation values. This method, grounded in station-based data, is applied seven times using climate projections for the Karaisali station under both historical and future scenarios from the best-performing MMEs. As a result, projections of monthly net lake evaporation are produced for the historical baseline period (1969–2014), as well as for the 25-year future periods (2025–2049, 2050–2074, and 2075–2099).

3.5 | Hydropower Production and Water Supply Under Climate Change Scenarios

Operational studies for the Karakuz HEPP are conducted using a multi-purpose reservoir operation macro developed in Visual Basic for Applications (VBA). The monthly operational algorithm adopts a dual-level structure that first prioritizes water demand supply and then maximizes firm power production for 95% of the operational period, while the remaining storage capacity is used to enhance secondary power generation up to

the total installed capacity. At the beginning of each month, the algorithm evaluates the available reservoir storage and inflow to determine the total releasable volume. The operation follows a hierarchical allocation scheme in which water demands receive the highest priority. When available storage is insufficient to meet these demands, the resulting deficit is recorded as a monthly water-supply shortfall. Only the remaining storage after these priority releases is allocated for hydropower generation, subject to turbine capacity limits, minimum operating level, and spillway constraints.

Hydropower releases are determined through an iterative reliability routine designed to maintain firm power generation in at least 95% of the operational period. The process begins with an initial estimate of firm discharge, which is tested against the entire operational period. If this discharge cannot be sustained with the required reliability, it is progressively reduced until the 95% reliability criterion is met. The resulting value defines the firm release, ensuring dependable energy generation even under dry conditions. Any discharge above this threshold constitutes a surplus release, representing secondary energy production. This dual-level framework safeguards essential water demand releases while balancing firm energy reliability with opportunities to maximize total energy generation.

The topographic and technical characteristics of the Karakuz Dam and HEPP are incorporated as fixed inputs. Topographic features are represented through reservoir volume-elevation and area-elevation curves (Figure S1d). Technical specifications, obtained from the project feasibility report (Dolsar 2008), include reservoir operating levels, penstock and power tunnel dimensions, design discharge, turbine details, tailwater level, efficiency curves, and spillway capacity. Climate-dependent input variables include monthly mean inflows to the reservoir and monthly net lake evaporations per unit area. In all runs, the starting reservoir volume is established as equivalent to the total capacity, while the final storage volume is constrained to ensure full utilization of active storage for power generation.

Historical operations (1969–2014) are first simulated using monthly average inflows derived from SGS records, along with monthly net lake evaporation rates calculated using observed precipitation and temperature data from the Karaisali station. This run is then repeated using historical inflow estimates simulated by the calibrated SWAT model, along with monthly net lake evaporation rates derived under the historical experiment. Future reservoir operations are conducted over the 2025–2049, 2050–2074, and 2075–2099 periods using SWAT-based simulated monthly average inflows and projected monthly net lake evaporation rates for each SSP scenario.

In each operational run, the algorithm prioritizes a continuous release of 0.1 m^3/s to support the Korkun Creek ecosystem and a transfer of 0.4 m^3/s to meet the planned water supply for Nevsehir province (Dolsar 2008). Applying constant environmental and domestic water allocations across both historical and future periods ensures that variations in hydropower performance can be attributed solely to climatic changes, rather than to the difficult-to-formulate future water use assumptions. Although this simplification may underestimate potential increases in water demand, it provides a consistent basis for assessing the relative vulnerability of hydropower production under the SSP2-4.5 and SSP5-8.5 scenarios.

4 | Results and Discussion

4.1 | Future Changes in Precipitation and Temperature

The basin-wide performance metrics and model rankings, computed based on the basin coverage ratios of the Nigde and Karaisali MSs under the application of the LS, DM, and QM bias correction methods, are presented in Tables S2–S4, respectively. For each climate variable, the top four ranked GCMs in the basin-specific evaluation are selected as MME members. Accordingly, for the precipitation variable, the ensemble members under the LS method are FGOALS-g3, GFDL-CM4, CanESM5, and CMCC-ESM2; under the DM method, CMCC-ESM2, TaiESM1, INM-CM4-8, and FGOALS-g3; and under the QM method, EC-Earth3-CC, EC-Earth3-Veg, MIROC6, and CMCC-ESM2. For temperature, the ensemble members under the LS method are MPI-ESM1-2-HR, NorESM2-LM, FGOALS-g3, and NorESM2-MM, while under the DM method, the selected GCMs are MPI-ESM1-2-HR, GFDL-CM4, NorESM2-LM, and MRI-ESM2-0.

Daily climate projections of the MMEs for the historical experiment and future pathway scenarios are generated by applying arithmetic averaging to the bias-adjusted outputs of the ensemble members at each station coordinate. The basin-wide efficacy metrics of the ensembles constructed using different bias correction methods under the historical experiment are comparatively assessed to identify the most effective bias adjustment technique and, accordingly, the best-performing MME for each climate variable. Table 1 presents the performance statistics of the MMEs formed using the LS, DM, and QM methods. In this table, MD, KGE, and FSS values closest to 1, as well as nRMSE values closest to 0, indicate the highest-performing MME. Accordingly, the LS method achieves the highest performance compared to the DM and QM methods based on the MD, nRMSE, and FSS metrics for precipitation, whereas the DM method exhibits higher or comparable performance to the LS method based on the MD, nRMSE, and KGE metrics for maximum temperature and the MD, KGE, and FSS metrics for minimum temperature. Based on these results, both methods outperform the other bias correction methods in three of the four applied evaluation metrics; the LS method is identified as the most effective technique for the precipitation variable, while the DM method yields the best performance for the temperature variables.

The statistical performance of precipitation simulations produced by the best-performing MME, composed of FGOALS-g3, GFDL-CM4, CanESM5, and CMCC-ESM2, is not entirely satisfactory, especially with the MD and KGE metrics. Comparable outcomes are evident in other studies that use different bias adjustment and ensemble averaging methods to produce projections based on MMEs (e.g., Ahmed et al. 2019; Bağçaci et al. 2021; Seker and Gumus 2022). These findings consistently indicate that the ability of CMIP6 GCMs to simulate precipitation is generally inferior to their performance in simulating temperature. Nevertheless, for the best-performing MMEs, both precipitation

TABLE 1 | Performance metrics of the MME means.

Climate variable	Bias correction	Member GCMs	MD	nRMSE	KGE	FSS
Precipitation	LS	FGOALS-g3	0.543	0.156	0.459	0.828
		GFDL-CM4				
		CanESM5				
		CMCC-ESM2				
	DM	CMCC-ESM2	0.543	0.165	0.475	0.808
		TaiESM1				
		INM-CM4-8				
		FGOALS-g3				
	QM	EC-Earth3-CC	0.512	0.169	0.431	0.802
		EC-Earth3-Veg				
		MIROC6				
		CMCC-ESM2				
Maximum temperature	LS	MPI-ESM1-2-HR	0.887	0.064	0.958	0.994
		NorESM2-LM				
		FGOALS-g3				
		NorESM2-MM				
	DM	MPI-ESM1-2-HR	0.890	0.064	0.962	0.992
		GFDL-CM4				
		NorESM2-LM				
		MRI-ESM2-0				
Minimum temperature	LS	MPI-ESM1-2-HR	0.887	0.061	0.950	0.981
		NorESM2-LM				
		FGOALS-g3				
		NorESM2-MM				
	DM	MPI-ESM1-2-HR	0.890	0.062	0.955	0.981
		GFDL-CM4				
		NorESM2-LM				
		MRI-ESM2-0				

and temperature estimates generated under the historical scenario align well with seasonal and annual averages recorded at the synoptic stations (Table 2). For the historical analysis period between 1969 and 2014, the average annual daily rainfall rates measured at the Nigde and Karaisali MSs are 0.91 and 2.35 mm, respectively. For the same period and locations, the corresponding simulations from the best-performing MME estimate the mean annual daily total precipitation as 0.91 and 2.38 mm, respectively. With respect to temperature, the observed average annual maximum/minimum temperatures during 1969–2014 are 17.53°C/5.22°C at Nigde and 24.19°C/13.98°C at Karaisali. For the same period, the MME composed of MPI-ESM1-2-HR, GFDL-CM4, NorESM2-LM, and MRI-ESM2-0 simulates the average annual maximum/minimum temperatures as 17.54°C/5.23°C for Nigde and 24.17°C/14.02°C for Karaisali.

Climate projections generated by the best-performing MMEs under the pathway scenarios are analyzed based on seasonal and annual averages across the near- (2025–2049), mid- (2050–2074), and late-century (2075–2099) periods using the averages achieved under the historical scenario as the reference (Table 2). Under the mid-forcing SSP2-4.5 scenario, the greatest reductions in average annual daily total rainfall magnitude for the coordinates of the Nigde and Karaisali stations are projected for the mid-century period, with decreases of 4.4% and 5.9%, respectively. At the Nigde MS, summer and autumn precipitation during the mid-century are expected to decrease by 10.5% and 15.4%, respectively, while autumn precipitation in the late-century is estimated to decrease by 14.1%. At the Karaisali MS, summer and autumn precipitation are predicted to decline by 12.8% and 13.7% during 2050–2074, and by 11.5% and 12.6%

TABLE 2 | Seasonal and annual precipitation and temperature statistics for the Nigde and Karaisali stations under the CMIP6 historical experiment and future scenarios SSP2-4.5 and SSP5-8.5.

Climate data		CMIP6 historical experiment (observed)	SSP2-4.5			SSP5-8.5		
Analysis period		1969–2014	2025–2049	2050–2074	2075–2099	2025–2049	2050–2074	2075–2099
Nigde MS								
Mean precipitation (mm/day)	Autumn	0.78 (0.79)	0.74	0.66	0.67	0.66	0.64	0.54
	Winter	1.16 (1.11)	1.14	1.08	1.13	1.06	1.08	0.98
	Spring	1.35 (1.36)	1.36	1.38	1.41	1.29	1.35	1.24
	Summer	0.38 (0.39)	0.38	0.34	0.36	0.37	0.36	0.34
	Annual	0.91 (0.91)	0.9	0.87	0.89	0.84	0.86	0.77
Mean maximum temperature (°C)	Autumn	19.21 (19.27)	21.39	21.98	22.97	21.89	23.79	25.87
	Winter	5.97 (5.93)	8.07	9.33	10.31	8.79	11.07	13.23
	Spring	16.54 (16.48)	18.04	18.85	19.55	18.53	20.31	22.8
	Summer	28.24 (28.24)	30.63	31.62	32.16	30.89	33.03	35.31
	Annual	17.54 (17.53)	19.58	20.49	21.3	20.08	22.1	24.35
Mean minimum temperature (°C)	Autumn	5.88 (5.91)	7.59	8.22	8.94	8	9.45	11.08
	Winter	−3.51 (−3.57)	−2.01	−1.26	−0.68	−1.72	−0.38	0.69
	Spring	4.49 (4.45)	5.68	6.16	6.61	5.91	6.99	8.49
	Summer	13.89 (13.94)	16.01	16.89	17.37	16.19	18.02	19.96
	Annual	5.23 (5.22)	6.86	7.54	8.1	7.13	8.56	10.1
Karaisali MS								
Mean precipitation (mm/day)	Autumn	1.83 (1.80)	1.72	1.58	1.6	1.58	1.51	1.32
	Winter	4.30 (4.10)	4.2	4.02	4.19	3.94	3.92	3.58
	Spring	2.63 (2.69)	2.63	2.69	2.7	2.53	2.64	2.37
	Summer	0.78 (0.81)	0.76	0.68	0.69	0.72	0.69	0.66
	Annual	2.38 (2.35)	2.32	2.24	2.29	2.18	2.18	1.98
Mean maximum temperature (°C)	Autumn	26.83 (26.90)	28.76	29.34	30.19	29.26	30.93	32.76
	Winter	14.22 (14.28)	15.56	16.4	16.99	16.06	17.52	18.96
	Spring	22.26 (22.21)	23.64	24.37	25.02	24.09	25.71	27.85
	Summer	33.22 (33.19)	35.13	35.93	36.33	35.38	37	38.74
	Annual	24.17 (24.19)	25.81	26.55	27.17	26.24	27.83	29.62
Mean minimum temperature (°C)	Autumn	15.98 (15.97)	17.56	18.14	18.74	17.93	19.2	20.66
	Winter	6.42 (6.39)	7.31	7.78	8.12	7.54	8.31	9.02
	Spring	12.09 (12.00)	13.24	13.71	14.15	13.45	14.57	15.92
	Summer	21.47 (21.42)	23.34	24.08	24.45	23.46	24.98	26.54
	Annual	14.02 (13.98)	15.39	15.96	16.4	15.63	16.8	18.07

during 2075–2099. The mean annual maximum/minimum temperatures at Nigde and Karaisali are projected to gradually rise, reaching 3.76°C/2.87°C and 3.00°C/2.38°C, respectively, by the late-century.

Under SSP5-8.5, the impacts of climate change become more pronounced compared to SSP2-4.5 (Table 2). At the Nigde MS, the average annual daily total rainfall is projected to decrease by 7.7%, 5.5%, and 15.4% during 2025–2049, 2050–2074, and 2075–2099, respectively. At the Karaisali MS, the corresponding decreases are 8.4%, 8.4%, and 16.8%. For Nigde, autumn precipitation is expected to decline by 15.4%, 17.9%, and 30.8% across the near-, mid-, and late-century periods, respectively. During the late-century, winter and summer precipitation are projected to fall by 15.5% and 10.5%, respectively. For Karaisali, autumn precipitation is predicted to decrease by 13.7% during the near-century period. In the mid-century, reductions of 11.5% in summer and 17.5% in autumn are projected, while in the late-century, summer, autumn, and winter precipitation are expected to decline by 15.4%, 27.9%, and 16.7%, respectively. In terms of temperature anomalies, the average annual maximum/minimum temperatures at the Nigde and Karaisali station coordinates are projected to gradually increase, reaching 6.81°C/4.87°C and 5.45°C/4.05°C, respectively, by the late-century.

4.2 | Performance Evaluation of SWAT

The SWAT model calibration is performed against the monthly mean streamflow rates of Korkun Creek at the dam site, derived by transposing the extended monthly average flow data from the Karakuz SGS to the dam site. This streamflow time series for the 1969–2014 period serves as the observed inflow data for the Karakuz reservoir. Inflow data from 1969 to 1998 are used for model calibration, while data from 1999 to 2014 are used for model validation. The performance evaluation is conducted using five key metrics: P-factor, R-factor, NSE, PBIAS, and RSR. For runoff simulations, a P-factor exceeding 0.7 combined with an R-factor below 1.5 is generally regarded as indicative of satisfactory model performance, depending on the spatial scale of the modeling basin and the quality of input data used for model setup and calibration (Abbaspour 2015). Regarding NSE, PBIAS, and RSR, the model is considered to perform satisfactorily for monthly streamflow simulations when the NSE exceeds 0.5, PBIAS remains within ±15%, and RSR is below 0.7 (Moriasi et al. 2007, 2015).

Table S5 outlines the sensitive parameters incorporated into the calibration procedure, detailing their calibrated ranges and best-performing rates, listed in descending order of sensitivity for each stage. For the calibration period, Figure 3a shows the monthly average inflow values derived from the SGS data (i.e., observed), the 95PPU band simulated by the calibrated model, and the monthly average streamflow values from the best simulation. The last combined run, conducted using the calibrated parameter intervals, resulted in a P-factor of 0.81 and an R-factor of 1.02. The simulation achieving the highest objective function value in this iteration produces NSE, PBIAS, and RSR values of 0.64, 14.4%, and 0.60, respectively, designating that the model performs satisfactorily under the best-performing parameter set.

To validate the calibrated parameter ranges, a combined iteration is conducted using the same intervals against the historical inflows of the Karakuz reservoir for the 1999–2014 period, based on the SGS measurements. The resulting P-factor and R-factor from this iteration are 0.79 and 1.52, respectively. The 95PPU band corresponding to the validation period is illustrated in Figure 3b. The best-performing parameter set is also verified over the period 1999–2014. Figure 3b presents the corresponding monthly average simulated values (i.e., best simulation), along with the historical inflows of the Karakuz reservoir, to graphically compare the simulation performance. The NSE, PBIAS, and RSR values for this simulation are 0.63, −5.6%, and 0.61, respectively. The attained metrics for validation indicate that the simulation performance using the best-performing parameter set is comparable to that of the calibration period, confirming that the model exhibits robust and acceptable performance across both periods.

Although the SWAT model demonstrates satisfactory overall performance, a closer examination of Figure 3a,b reveals that the simulated monthly time series tend to underestimate some peak runoff events during the calibration period and slightly overestimate some low flows during the validation period. These discrepancies indicate that, while the model is capable of reproducing monthly mean streamflow dynamics, it shows partial inconsistencies in representing high- and low-flow conditions.

4.3 | Future Changes in Streamflow Regime

To simulate monthly mean streamflow rates at the reservoir site on Korkun Creek for the historical 1969–2014 period and the three future 25-year intervals between 2025 and 2099, the SWAT model is executed using the best-performing parameter set by inputting daily precipitation and temperature projections derived from the best-performing MMEs under the CMIP6 historical experiment and the future SSP2-4.5 and SSP5-8.5 pathway scenarios for the Nigde and Karaisali station locations. The seasonal and annual averages of the inflow projections generated by the SWAT simulations are presented in Table 3.

Accordingly, the average streamflow values at the reservoir site derived from the SGS records for the 1969–2014 period are calculated as 3.86 m^3/s for autumn, 7.31 m^3/s for winter, 14.35 m^3/s for spring, 6.21 m^3/s for summer, and 7.93 m^3/s annually. In comparison, the SWAT model simulations driven by the MME projections under the CMIP6 historical experiment produce corresponding average streamflow rates of 3.58, 6.88, 14.73, 6.81, and 8.00 m^3/s, respectively. The close agreement between the SGS-derived and model-simulated flow values supports both the reliability of the best-performing MME projections and the success of the calibration. Accordingly, potential alterations in the flow regime of Korkun Creek at the Karakuz Dam site are examined for the SSP2-4.5 and SSP5-8.5 pathway scenarios, employing streamflow estimates from the CMIP6 historical experiment as the reference baseline.

Under SSP2-4.5, the mean annual streamflow at the reservoir site is projected to decrease by 16.6%, 16.2%, and 13.9% in the near-, mid-, and end-century intervals, respectively. In all three future periods, summer flows are expected to

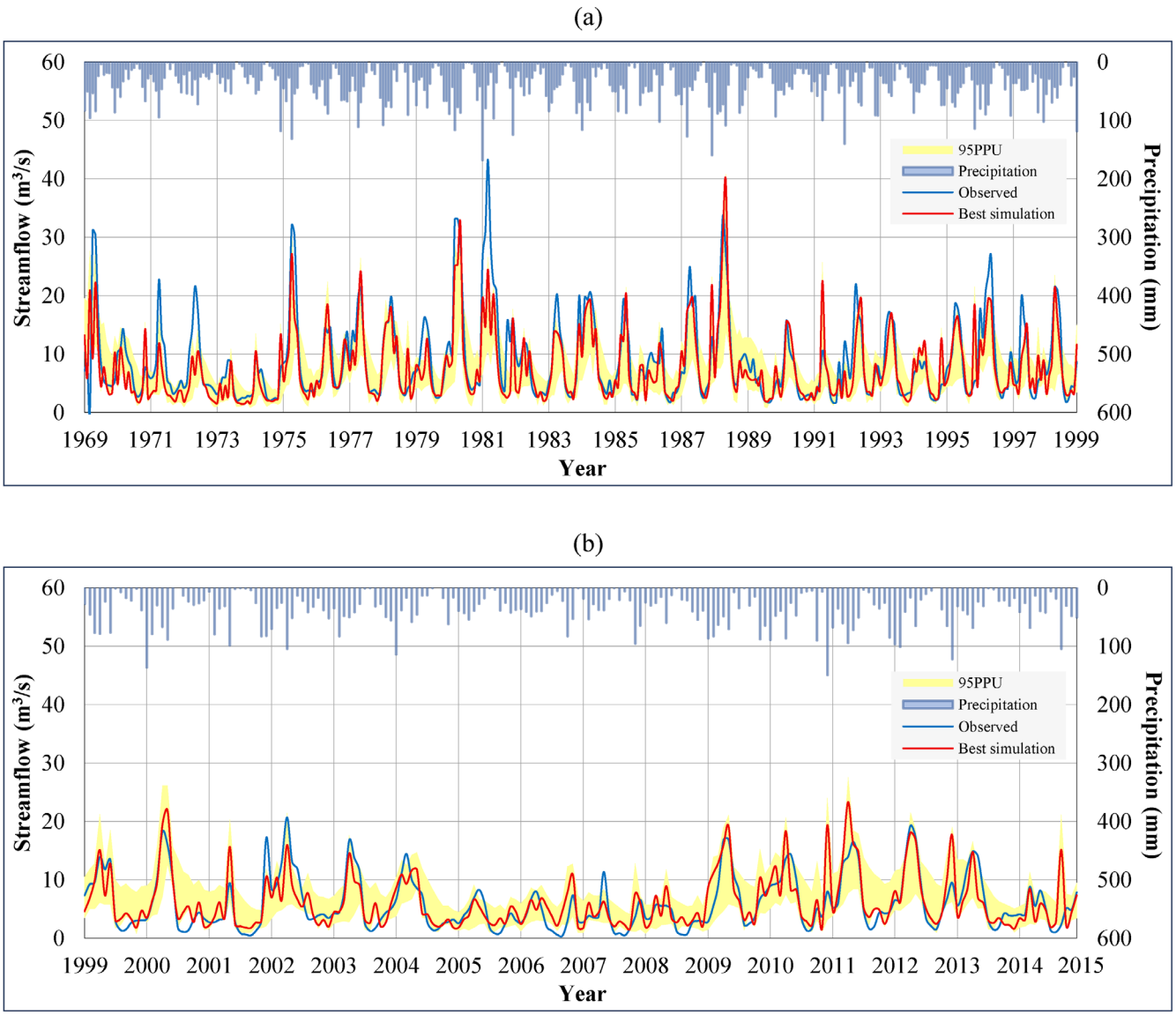

FIGURE 3 | Monthly mean streamflow simulations of the calibrated SWAT model at the Karakuz Dam location for the (a) calibration and (b) validation periods.

decline by approximately 30%, while spring and autumn flows are projected to decrease by 15%–20%. Although future rainfall projections for the spring and winter months at both the Nigde and Karaisali MSs do not indicate significant changes compared to the 1969–2014 period, the simulated reductions in spring flows across all future periods and the increases in winter flows during the mid- and end-century periods suggest a shift in precipitation phase (Tables 2 and 3). The evidence indicates that snow accumulation may be replaced by rainfall during the second half of the century.

The projected streamflow reductions under the SSP5-8.5 scenario are substantially greater than those under SSP2-4.5. Average annual flows during 2025–2049, 2050–2074, and 2075–2099 are projected to be 27.7%, 24.9%, and 44.5% lower, respectively, than the historical average. In the near- and mid-century, the projected declines in average streamflow reach 33.3% and 30.5% in spring, 36.3% and 39.9% in summer, and 25.1% and 27.7% in autumn, respectively. For winter, a decrease of 8.8% is projected for the near-century period, while a 3.4% increase is expected in the mid-century. The period with the most pronounced streamflow reduction under this scenario is foreseen to be the end-century, during which spring, summer, autumn, and winter flows are expected to decline by 54.4%, 54.3%, 41.3%, and 15.2%, respectively. As in SSP2-4.5, the anticipated low streamflow changes for the winter months are likely due to a shift from snowfall to rainfall in future winters, driven by rising temperatures (Tables 2 and 3).

4.4 | Future Changes in Lake Evaporation

The mean annual net evaporation from the Karakuz reservoir is estimated to be 553.57 mm, based on mean monthly precipitation and temperature measurements from the Karaisali MS between 1969 and 2014. When the evaporation calculation is repeated using the best-performing MME projections under the CMIP6 historical experiment at the Karaisali station

TABLE 3 | Seasonal and annual inflow and net lake evaporation statistics for the Karakuz reservoir under the CMIP6 historical experiment and future scenarios SSP2-4.5 and SSP5-8.5.

Climate data	CMIP6 historical experiment (observed)	SSP2-4.5			SSP5-8.5		
Analysis period	**1969–2014**	**2025–2049**	**2050–2074**	**2075–2099**	**2025–2049**	**2050–2074**	**2075–2099**
Mean inflow (m^3/s)							
Autumn	3.58 (3.86)	3.01	2.87	2.87	2.68	2.59	2.10
Winter	6.88 (7.31)	6.93	7.25	7.82	6.27	7.11	5.83
Spring	14.73 (14.35)	11.92	11.86	12.10	9.83	10.24	6.72
Summer	6.81 (6.21)	4.81	4.83	4.75	4.34	4.09	3.11
Annual	8.00 (7.93)	6.67	6.70	6.89	5.78	6.01	4.44
Mean total net lake evaporation (mm)							
Autumn	164.62 (168.83)	189.94	208.73	218.68	206.78	240.39	292.48
Winter	0.00 (0.00)	0.00	0.00	0.00	0.00	0.00	0.00
Spring	26.63 (28.31)	44.32	44.15	48.33	42.88	59.81	101.26
Summer	353.98 (356.42)	396.48	420.51	427.11	404.44	440.81	478.07
Annual	545.22 (553.57)	630.74	673.39	694.12	654.11	741.01	871.81

location, the average annual net lake evaporation is found to be 545.22 mm. Given the close agreement between the net evaporation values computed using the station records and those based on the MME projections, the calculation is extended to the future pathway scenarios (Table 3). Under SSP2-4.5, annual net lake evaporation is projected to increase to 630.74, 673.39, and 694.12 mm for the respective future periods of 2025–2049, 2050–2074, and 2075–2099. These increases are more obvious under SSP5-8.5, with annual net lake evaporation projected to reach 654.11, 741.01, and 871.81 mm over the same periods. The projected increases of up to 60% under the high-forcing SSP5-8.5 scenario underscore the influence of rising temperatures and reduced rainfall in the dam basin, even though evaporation from the water surface accounts for only a minor part of the reservoir's overall water budget.

4.5 | Future Changes in Hydropower Production and Water Supply

Reservoir operation results, obtained by inputting monthly average inflow projections and average monthly net lake evaporation estimates into the developed operational algorithm, are summarized in Table 4. For the historical period from 1969 to 2014, the operational analysis, conducted using lake evaporation rates based on synoptic MS data and inflows calculated from SGS measurements, yields a mean annual hydroelectricity generation potential of 290.34 GWh/year for the Karakuz HEPP. When monthly average inflow and net lake evaporation projections from the CMIP6 historical experiment are used for the same period, the estimated energy production increases to 313.95 GWh/year.

A comparison of these two operational runs for the historical analysis period shows that operation based on climate conditions under the CMIP6 historical experiment leads to a slight decrease in both the number and volume of spillway discharges, along with a modest increase in firm discharge and, consequently, in firm energy production. This outcome can be attributed to the SWAT model's suboptimal representation of high- and low-flow conditions. Consequently, although the general inflow regime and mean flow characteristics are well captured, this limitation affects the reservoir's operational dynamics, particularly during high-flow months. Despite these differences, both operational runs for the historical period produce similar total energy outputs and regulation ratios, and demonstrate that the municipal water demand of 0.4 m^3/s for Nevsehir province, as well as the environmental flow requirement of 0.1 m^3/s for Korkun Creek, are consistently met throughout the operational timeline.

According to analyses under the SSP2-4.5 scenario, average annual hydroelectricity generation capacity at the Karakuz HEPP is projected to decrease by 16.6%, 15.7%, and 14.3% in the 2025–2049, 2050–2075, and 2075–2099 periods, respectively, compared to the results under the historical experiment. These foreseen decreases in energy production correspond to the anticipated reductions in reservoir inflows. The evidence suggests that the noticeable reduction in both the frequency and volume of spillway discharges under future climate conditions has only a limited impact on overall energy production. In addition, no notable change is observed in the regulation ratios for the future periods relative to the historical period. Therefore, the expected inflow reductions of 16.6%, 16.2%, and 13.9% in the near-, mid-, and end-century periods, respectively, are expected to have a direct effect on hydroelectricity generation (Tables 3 and 4).

TABLE 4 | Operational statistics for the Karakuz Dam and HEPP Project under the CMIP6 historical experiment and future scenarios SSP2-4.5 and SSP5-8.5.

Climate data		CMIP6 historical experiment (observed)	SSP2-4.5			SSP5-8.5		
Analysis period		**1969–2014**	**2025–2049**	**2050–2074**	**2075–2099**	**2025–2049**	**2050–2074**	**2075–2099**
Inflow	m^3/s	8.00 (7.93)	6.67	6.70	6.89	5.78	6.01	4.44
	$hm^3/year$	252.09 (250.03)	209.88	211.08	216.78	182.04	188.99	139.72
Lake evaporation	$hm^3/year$	0.21 (0.20)	0.25	0.26	0.27	0.25	0.29	0.33
Domestic water supply	$hm^3/year$	12.62 (12.62)	12.62	12.62	12.62	12.62	12.62	12.62
	%	100.0 (100.0)	100.0	100.0	100.0	100.0	100.0	100.0
Environmental water supply	$hm^3/year$	3.16 (3.16)	3.16	3.16	3.16	3.16	3.16	3.16
	%	100.0 (100.0)	100.0	100.0	100.0	100.0	100.0	100.0
Spillway release	month	32 (51)	5	5	6	0	3	1
	m^3/s	1.90 (6.03)	1.17	0.47	3.32	0.00	1.46	0.79
	$hm^3/year$	3.47 (17.55)	0.62	0.25	2.10	0.00	0.46	0.08
Power release	m^3/s	7.38 (6.87)	6.14	6.19	6.31	5.28	5.49	3.93
	$hm^3/year$	232.71 (216.58)	193.37	194.93	198.77	166.15	172.61	123.67
Firm discharge	m^3/s	3.06 (1.97)	2.60	2.61	2.51	2.35	2.28	1.86
Regulation ratio	%	92.3 (86.6)	92.1	92.3	91.7	91.3	91.3	88.5
Firm energy	GWh/year	124.36 (79.29)	105.52	105.73	101.70	94.87	92.26	74.36
Secondary energy	GWh/year	189.59 (211.05)	156.47	159.04	167.30	131.02	141.94	93.14
Total energy	GWh/year	313.95 (290.34)	261.99	264.77	269.00	225.89	234.19	167.50

Under SSP5-8.5, the reduction in hydroelectricity production is considerably greater than under SSP2-4.5 across all three future periods. Specifically, average annual energy generation is projected to decrease by 21.8%, 18.9%, and 42.0%, respectively, in the near-, mid-, and end-century intervals, relative to the production under the CMIP6 historical experiment. Despite an almost complete elimination of spillway discharges, the projected inflow reductions of 27.7%, 24.9%, and 44.5% over the respective periods still result in substantial losses in hydroelectricity production (Tables 3 and 4).

When seasonal variations in hydropower production are examined in Figure 4, the results indicate substantial declines in firm energy generation across all seasons under both pathway scenarios. Under SSP2-4.5, firm energy generation in autumn, winter, spring, and summer is projected to decrease by 17.4%–22.0%, 12.1%–15.9%, 13.1%–16.5%, and 15.5%–19.1%, respectively. Under SSP5-8.5, these seasonal reductions intensify, reaching 28.7%–42.6% in autumn, 21.2%–39.8% in winter, 21.1%–36.9% in spring, and 24.7%–41.9% in summer over the considered 25-year future periods. Firm energy declines substantially across seasons, yet the magnitude of these changes remains relatively consistent among seasons, while secondary energy production shows a more substantial seasonal response.

Secondary energy displays stronger seasonal sensitivity, particularly under the high-forcing pathway scenario. Under SSP2-4.5, secondary energy is projected to decline by 25.3%–27.2% in autumn, 16.6%–17.3% in spring, and 46.2%–47.1% in summer. Under SSP5-8.5, the projected reductions increase markedly to 28.4%–61.0% in autumn, 29.4%–57.8% in spring, and 54.1%–76.7% in summer. Winter exhibits a distinct response that differs from other seasons due to expected changes in the snow regime within the Karakuz basin. Under SSP2-4.5, winter secondary energy production is projected to increase by 13.6%, 20.4%, and 41.9% during the 2025–2049, 2050–2074, and 2075–2099 periods, respectively. Under SSP5-8.5, winter secondary energy shows comparatively small deviations from the historical period (1969–2014) for 2025–2049 and 2075–2100, with a 25.3% increase projected only for 2050–2074.

Consequently, total seasonal energy production at the Karakuz Project is expected to decline in most seasons. Under SSP2-4.5, seasonal mean total energy production is projected to decline by 19.1%–22.7% in autumn, 16.2%–16.6% in spring, and 31.5%–33.0% in summer, while winter totals are projected to increase moderately by 0.4%–14.1%. Under SSP5-8.5, total energy production is projected to decrease by 28.7%–46.4% in autumn, 28.1%–53.2% in spring, and 39.8%–59.7% in summer, whereas winter totals show mixed changes of −10.1%, +1.8%, and −18.9% in the 2025–2049, 2050–2074, and 2075–2099 periods, respectively.

As detailed annually in Table 4 and seasonally in Figure 4, the projected variations in spillway releases and lake evaporation amounts are insufficient to exert a discernible influence on the reservoir water balance. Taken together, these findings indicate that climate-induced inflow reductions will substantially limit the hydropower performance of the Karakuz HEPP in the future periods, particularly under the SSP5-8.5 scenario. On the other hand, for both climate scenarios and across all future periods, the operational results indicate that the designated flow rates of 0.4 m^3/s for domestic water supply and 0.1 m^3/s for ecological continuity are reliably supplied (Table 4). However, regardless of the scenario considered, it is evident that the anticipated economic benefits of the project, originally designed based on historical hydro-meteorological conditions, may not be achievable in the coming decades due to climate-driven changes across the watershed.

While inflow remains the principal determinant of hydropower generation, the reliability of forward-looking energy production assessments ultimately depends on the fidelity of streamflow projections. During the historical period (1969–2014), SWAT-simulated streamflow demonstrates strong agreement with observed discharge, and this consistency enables operational simulations driven by observation-based and model-based inflows to show close agreement. This validates the statistical rigor of the bias-correction framework, the representativeness of the selected GCM ensemble, and the satisfactory performance of the calibrated SWAT model. These alignments indicate that key hydro-climatic sensitivities, including seasonal flow timing and intra-annual variability, are credibly reproduced within the Karakuz basin. Therefore, the derived MME projections provide a robust decision-support foundation for quantifying hydropower vulnerability and informing long-term risk management.

Although uncertainties in GCM outputs are reduced through the MME approach, enabling calibrated SWAT simulations and subsequent operational runs to closely reproduce historical streamflow and hydropower performance with limited uncertainty transmission across the climate-hydrology-operations chain, future climate uncertainty still warrants further investigation. To evaluate projection robustness under SSP2-4.5 and SSP5-8.5, annual mean precipitation and temperature time series from all 24 GCMs are analyzed on a basin scale using the LS and DM methods for statistical downscaling, respectively, consistent with the bias adjustment procedure applied for the best-performing MMEs. Accordingly, as presented in Figure 5, despite inter-model structural divergence, the comparatively narrow 95% confidence intervals closely follow the annual mean precipitation, maximum temperature, and minimum temperature outcomes of the best-performing MMEs. This convergence attained for both SSP scenarios suggests that projected inflow reductions result from multi-model consensus rather than stochastic outliers, increasing confidence in future operational performance estimates.

Projected reductions in inflow and hydropower production in the Karakuz Dam are consistent with regional hydroclimatic responses reported for the Mediterranean basins, indicating that the project is not a hydrological outlier under warming (e.g., Gorguner and Kavvas 2020; Garcia et al. 2024; Yalcin 2024; Doğan and Şensoy 2025; Amaranto et al. 2025). The Mediterranean region is recognized as a climate-change hotspot, where strong seasonality, limited natural storage, and increasing water demand already drive severe water scarcity. Future warming, altered precipitation, and heightened drought exposure are expected to further reduce runoff and reservoir yields in the Mediterranean (Cherif et al. 2020; Ali et al. 2022). Within this context, Karakuz represents a typical medium-sized basin dependent on seasonal storage for water and energy supply. Despite future increases in regulation ratios from nearly

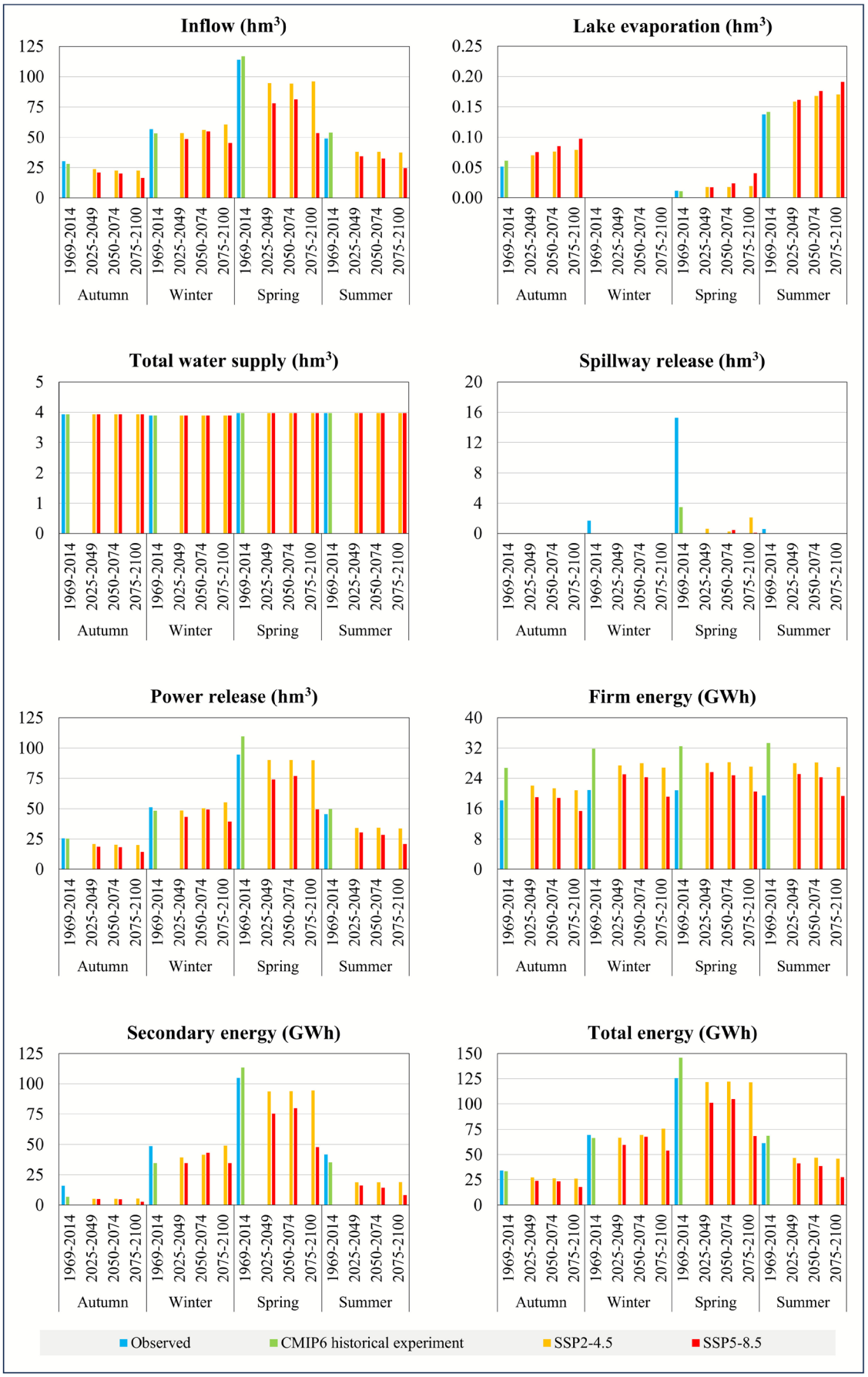

FIGURE 4 | Seasonal operational results for the Karakuz Dam and HEPP Project under the CMIP6 historical experiment and future scenarios SSP2-4.5 and SSP5-8.5.

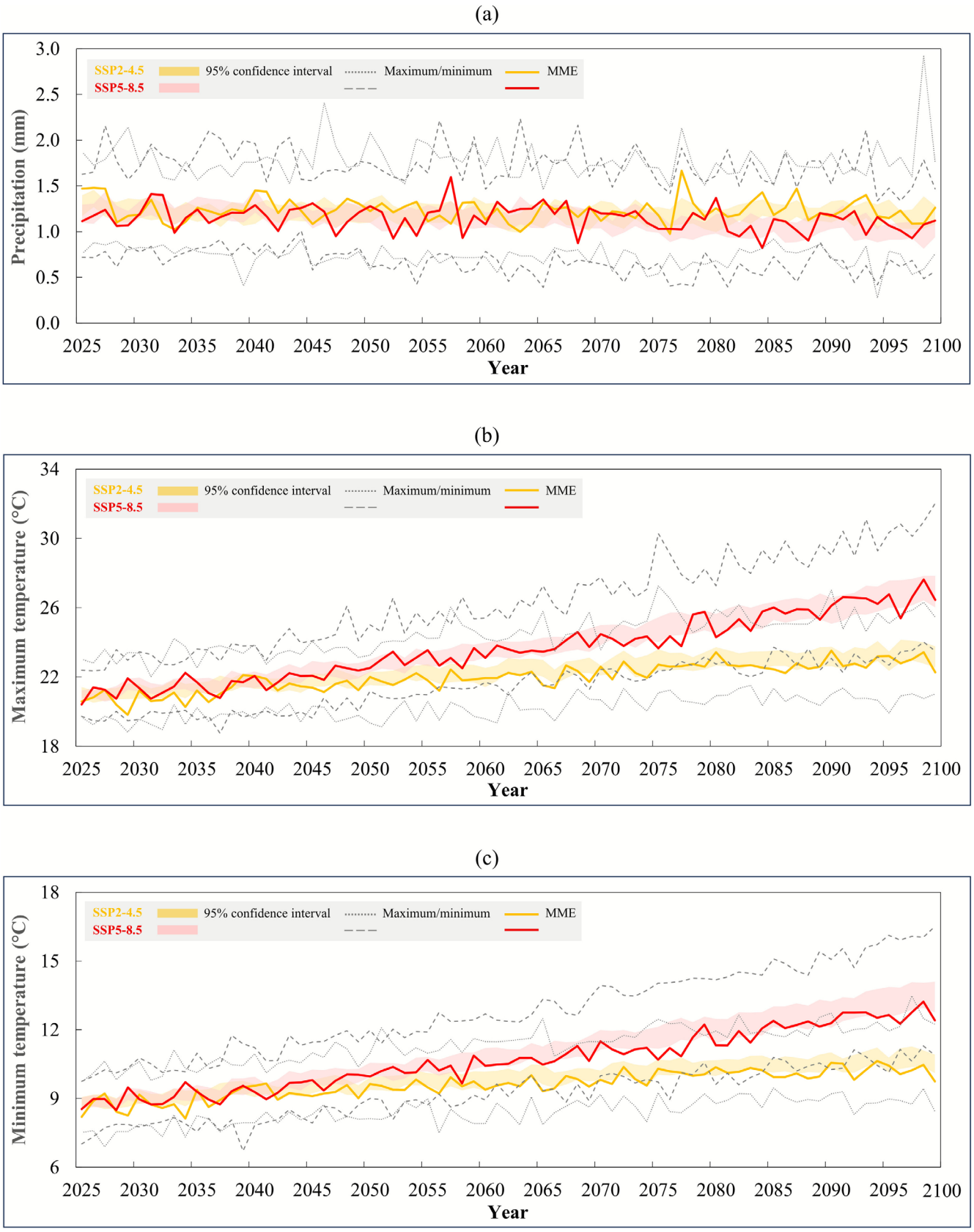

FIGURE 5 | Comparison of the bias-corrected annual mean time series from the 24 CMIP6 GCMs and the MMEs derived from the four best-performing GCMs over the Karakuz basin under the SSP2-4.5 and SSP5-8.5 scenarios: (a) precipitation, (b) maximum temperature, and (c) minimum temperature.

86% to 92%, hydropower generation is projected to decline by up to 46.6%, reflecting increasing operational stress (Table 4). Hundreds of dams in Turkey and other riparian countries operate under comparable hydrological constraints, yet most were designed using historical climate data, and planning studies for new dams continue to overlook the potential impacts of climate change (Yalcin 2024). The Karakuz results therefore emphasize the need for institutionalized, climate-responsive design and operation to support proactive adaptation across the region.

Hence, to enhance the adaptive capacity of the Karakuz Project under the projected climatic variability, both operational and structural interventions are necessary. On the operational side, dynamically optimized reservoir rule curves can be applied to adjust storage allocations and release schedules in response to altered inflow regimes, using real-time hydrometeorological monitoring and ensemble climate forecasts. Stochastic optimization techniques and scenario-based planning can be employed to manage uncertainties in precipitation and runoff projections. Structurally, increasing reservoir storage capacity or installing additional turbine units, where hydrological, environmental, and economic constraints allow, can improve system flexibility and energy generation potential under variable climatic conditions. However, such structural interventions require comprehensive feasibility assessments that integrate cost–benefit analyses to quantify economic efficiency, environmental impact evaluations to assess potential effects on aquatic and terrestrial ecosystems, and regulatory compliance reviews to ensure consistency with national water management and environmental protection frameworks. These assessments are essential to ensure that structural adaptive measures achieve sustainable and balanced outcomes under changing climatic conditions.

5 | Conclusion

This study evaluates whether the expected contributions of water resources projects located in the Mediterranean region, one of the most prominent global warming hotspots, can continue to be sustained in terms of water supply and hydropower production in the coming decades, using the Karakuz Dam and HEPP Project as a case study. The operational analyses conducted indicate that adaptation measures must be implemented to address changing climate conditions. The anticipated variations in the hydro-climatic regime of the dam catchment could lead to substantial declines in average annual hydroelectricity generation, reaching up to 16.6% and 46.6% for the SSP2-4.5 and SSP5-8.5 pathway scenarios, respectively. Even with these challenges, the results of operational studies under both future scenarios show that the domestic water demand of Nevsehir province, along with the environmental flow requirement of Korkun Creek, can still be met consistently throughout the century, assuming that the project's water supply objectives remain unchanged; however, future increases in water demand are inevitable.

Owing to the partial inadequacy of the calibrated SWAT model in simulating high- and low-flow conditions, reservoir operations based on inflow projections do not produce consistent outcomes in terms of spillway utilization and firm energy generation statistics. Therefore, future studies are advised to incorporate high-resolution spatial datasets into the hydrological model setup and to explore alternative bias adjustment and averaging methods for precipitation data from GCMs. Such improvements could enhance the alignment of streamflow projections with station-based observations and, hence, improve model reliability (Kim et al. 2016; Özcan et al. 2016; Wang et al. 2020). Furthermore, the applied methodology could be advanced by incorporating projected changes in additional climate variables, such as solar radiation, humidity, and wind speed, into both the runoff modeling process (Gorguner and Kavvas 2020) and the estimation of lake evaporation through lake-climate models (La Fuente et al. 2024). To conclude, the projections obtained in this study are expected to help raise awareness of the necessity for effective adaptation actions to ensure the long-term viability of hydropower projects in Mediterranean riparian countries in the decades ahead.

Author Contributions

Emrah Yalcin: conceptualization, methodology, software, data curation, investigation, validation, formal analysis, supervision, visualization, writing – original draft, writing – review and editing. **Cansu Boz:** software, investigation, formal analysis, visualization, writing – review and editing.

Disclosure

AI Usage Statement: The authors declare that no artificial intelligence (AI) tools were used for content generation, data analysis, or result interpretation in this study.

Conflicts of Interest

The authors declare no conflicts of interest.

Data Availability Statement

The data that support the findings of this study are available from the corresponding author upon reasonable request.

References

Abbaspour, K. C. 2015. *SWAT-CUP2: SWAT Calibration and Uncertainty Programs—A User Manual*. Eawag - Swiss Federal Institute of Aquatic Science and Technology.

Abbaspour, K. C., C. A. Johnson, and M. T. van Genuchten. 2004. "Estimating Uncertain Flow and Transport Parameters Using a Sequential Uncertainty Fitting Procedure." *Vadose Zone Journal* 3: 1340–1352. https://doi.org/10.2136/vzj2004.1340.

Abbaspour, K. C., E. Rouholahnejad, S. Vaghefi, R. Srinivasan, H. Yang, and B. Kløve. 2015. "A Continental-Scale Hydrology and Water Quality Model for Europe: Calibration and Uncertainty of a High-Resolution Large-Scale SWAT Model." *Journal of Hydrology* 524: 733–752. https://doi.org/10.1016/j.jhydrol.2015.03.027.

Abbaspour, K. C., J. Yang, I. Maximov, et al. 2007. "Modelling Hydrology and Water Quality in the Pre-Alpine/Alpine Thur Watershed Using SWAT." *Journal of Hydrology* 333: 413–430. https://doi.org/10.1016/j.jhydrol.2006.09.014.

Ahmed, K., D. A. Sachindra, S. Shahid, M. C. Demirel, and E.-S. Chung. 2019. "Selection of Multi-Model Ensemble of General Circulation Models for the Simulation of Precipitation and Maximum and Minimum Temperature Based on Spatial Assessment Metrics." *Hydrology and Earth System Sciences* 23: 4803–4824. https://doi.org/10.5194/hess-23-4803-2019.

Alarko (Alarko Holding). 2023. "The Karakuz Dam and HEPP Project." Accessed November 21, 2023. https://www.alarko.com.tr/en/projects/karakuz-dam-and-hepp/.

Ali, E., W. Cramer, J. Carnicer, et al. 2022. "Cross-Chapter Paper 4: Mediterranean Region." In *Climate Change 2022: Impacts, Adaptation and Vulnerability (Contribution of Working Group II to the Sixth Assessment Report of the Intergovernmental Panel on Climate Change)*, edited by H.-O. Pörtner, D. C. Roberts, M. Tignor, et al., 2233–2272. Cambridge University Press.

Almeida, M. P., O. Perpiñán, and L. Narvarte. 2015. "PV Power Forecast Using a Nonparametric PV Model." *Solar Energy* 115: 354–368. https://doi.org/10.1016/j.solener.2015.03.006.

Amaranto, A., L. Mancusi, F. Viterbo, R. Bonanno, G. Braca, and E. Garofalo. 2025. "Unravelling the Uncertainties in the Climate-Water-Energy Interplay: A Distributed Analysis of the Italian Territory." *Renewable Energy* 246: 122857. https://doi.org/10.1016/j.renene.2025.122857.

Arnold, J. G., J. R. Kiniry, R. Srinivasan, J. R. Williams, E. B. Haney, and S. L. Neitsch. 2013. *SWAT 2012 Input/Output Documentation*. Texas Water Resources Institute.

Bağçaci, S. Ç., I. Yucel, E. Duzenli, and M. T. Yilmaz. 2021. "Intercomparison of the Expected Change in the Temperature and the Precipitation Retrieved From CMIP6 and CMIP5 Climate Projections: A Mediterranean Hot Spot Case, Turkey." *Atmospheric Research* 256: 105576. https://doi.org/10.1016/j.atmosres.2021.105576.

Chen, W., Z. Jiang, and L. Li. 2011. "Probabilistic Projections of Climate Change Over China Under the SRES A1B Scenario Using 28 AOGCMs." *Journal of Climate* 24: 4741–4756. https://doi.org/10.1175/2011JCLI4102.1.

Cherif, S., E. Doblas-Miranda, P. Lionello, et al. 2020. "Drivers of Change." In *Climate and Environmental Change in the Mediterranean Basin—Current Situation and Risks for the Future (First Mediterranean Assessment Report)*, edited by W. Cramer, J. Guiot, and K. Marini, 59–180. Union for the Mediterranean Plan Bleu, UNEP/MAP.

Cos, J., F. Doblas-Reyes, M. Jury, R. Marcos, P.-A. Bretonnière, and M. Samsó. 2022. "The Mediterranean Climate Change Hotspot in the CMIP5 and CMIP6 Projections." *Earth System Dynamics* 13: 321–340. https://doi.org/10.5194/esd-13-321-2022.

Cygwin. 2022. "Cygwin User's Guide." Accessed May 20, 2022. https://www.cygwin.com/cygwin-ug-net/cygwin-ug-net.pdf.

Doğan, Y. O., and A. Şensoy. 2025. "Evaluation of Future Hydropower Potential for Mountainous Headwaters in Response to Climate Change." *Hydrological Sciences Journal* 70: 646–663. https://doi.org/10.1080/02626667.2025.2451160.

Dolsar (Dolsar Engineering Limited Company). 2008. *Upper Seyhan Korkun Basin—Karakuz Dam and Hydroelectric Power Plant Feasibility Report*. Dolsar Engineering Limited Company.

DSI (General Directorate of State Hydraulic Works). 2023. *Flow Gauging Yearbooks (1959–2015)*. GenPeral Directorate of State Hydraulic Works.

EC-JRC (European Commission—Joint Research Centre). 2006. "The Global Land Cover 2000 (GLC2000) Products." Accessed June 28, 2022. https://forobs.jrc.ec.europa.eu/products/glc2000/products.php.

ESGF (Earth System Grid Federation). 2022. "WCRP Coupled Model Intercomparison Project (Phase 6)." Accessed May 15, 2022. https://esgf-node.llnl.gov/projects/cmip6/.

Eyring, V., S. Bony, G. A. Meehl, et al. 2016. "Overview of the Coupled Model Intercomparison Project Phase 6 (CMIP6) Experimental Design and Organization." *Geoscientific Model Development* 9: 1937–1958. https://doi.org/10.5194/gmd-9-1937-2016.

FAO (Food and Agriculture Organization of the United Nations). 2007. "Digital Soil Map of the World (DSMW)." Accessed June 28, 2022. https://www.fao.org/geonetwork/srv/en/metadata.show?id=14116.

Garcia, X., L. Estrada, O. Llorente, and V. Acuña. 2024. "Assessing Small Hydropower Viability in Water-Scarce Regions: Environmental Flow and Climate Change Impacts Using a SWAT+ Based Tool." *Environmental Sciences Europe* 36: 126. https://doi.org/10.1186/s12302-024-00938-1.

Giorgi, F. 2006. "Climate Change Hot-Spots." *Geophysical Research Letters* 33: L08707. https://doi.org/10.1029/2006GL025734.

Gorguner, M., and M. L. Kavvas. 2020. "Modeling Impacts of Future Climate Change on Reservoir Storages and Irrigation Water Demands in a Mediterranean Basin." *Science of the Total Environment* 748: 141246. https://doi.org/10.1016/j.scitotenv.2020.141246.

Gudmundsson, L. 2022. "Package 'Qmap': Statistical Transformations for Post-Processing Climate Model Output." Accessed October 25, 2023. https://cran.r-project.org/web/packages/qmap/qmap.pdf.

Gupta, H. V., H. Kling, K. K. Yilmaz, and G. F. Martinez. 2009. "Decomposition of the Mean Squared Error and NSE Performance Criteria: Implications for Improving Hydrological Modelling." *Journal of Hydrology* 377: 80–91. https://doi.org/10.1016/j.jhydrol.2009.08.003.

Iturbide, M., J. M. Gutiérrez, L. M. Alves, et al. 2020. "An Update of IPCC Climate Reference Regions for Subcontinental Analysis of Climate Model Data: Definition and Aggregated Datasets." *Earth System Science Data* 12: 2959–2970. https://doi.org/10.5194/essd-12-2959-2020.

Jiménez-Navarro, I. C., P. Jimeno-Sáez, A. López-Ballesteros, J. Pérez-Sánchez, and J. Senent-Aparicio. 2021. "Impact of Climate Change on the Hydrology of the Forested Watershed That Drains to Lake Erken in Sweden: An Analysis Using SWAT+ and CMIP6 Scenarios." *Forests* 12: 1803. https://doi.org/10.3390/f12121803.

Jones, P. W. 1999. "First- and Second-Order Conservative Remapping Schemes for Grids in Spherical Coordinates." *Monthly Weather Review* 127: 2204–2210. https://doi.org/10.1175/1520-0493(1999)127<2204:FASOCR>2.0.CO;2.

Kim, J., V. Y. Ivanov, and S. Fatichi. 2016. "Climate Change and Uncertainty Assessment Over a Hydroclimatic Transect of Michigan." *Stochastic Environmental Research and Risk Assessment* 30: 923–944. https://doi.org/10.1007/s00477-015-1097-2.

La Fuente, S., E. Jennings, J. D. Lenters, et al. 2024. "Ensemble Modeling of Global Lake Evaporation Under Climate Change." *Journal of Hydrology* 631: 130647. https://doi.org/10.1016/j.jhydrol.2024.130647.

Legates, D. R., and G. J. McCabe. 1999. "Evaluating the Use of "Goodness-of-Fit" Measures in Hydrologic and Hydroclimatic Model Validation." *Water Resources Research* 35: 233–241. https://doi.org/10.1029/1998WR900018.

Liersch, S. 2003. "Dewpoint Estimation Programs: dew.exe and dew02.exe." Accessed July 2, 2022. https://swat.tamu.edu/software/.

Masia, S., J. Sušnik, S. Marras, S. Mereu, D. Spano, and A. Trabucco. 2018. "Assessment of Irrigated Agriculture Vulnerability Under Climate Change in Southern Italy." *Water* 10: 209. https://doi.org/10.3390/w10020209.

MGM (Turkish State Meteorological Service). 2023a. *Daily Precipitation, Maximum and Minimum Temperature, Solar Radiation, Wind Speed, and Relative Humidity Records of the Nigde Meteorological Station (Station ID: 17250)*. Turkish State Meteorological Service.

MGM (Turkish State Meteorological Service). 2023b. *Daily Precipitation, Maximum and Minimum Temperature, Solar Radiation, Wind Speed, and Relative Humidity Records of the Karaisali Meteorological Station (Station ID: 17936)*. Turkish State Meteorological Service.

MGM (Turkish State Meteorological Service). 2023c. *Long-Term All Parameters Bulletin for the Nigde Meteorological Station (Station ID: 17250)*. Turkish State Meteorological Service.

MGM (Turkish State Meteorological Service). 2023d. *Long-Term All Parameters Bulletin for the Karaisali Meteorological Station (Station ID: 17936)*. Turkish State Meteorological Service.

Michaelides, S., T. Karacostas, J. L. Sánchez, et al. 2018. "Reviews and Perspectives of High Impact Atmospheric Processes in the Mediterranean." *Atmospheric Research* 208: 4–44. https://doi.org/10.1016/j.atmosres.2017.11.022.

Moriasi, D. N., J. G. Arnold, M. W. Van Liew, R. L. Bingner, R. D. Harmel, and T. L. Veith. 2007. "Model Evaluation Guidelines for Systematic Quantification of Accuracy in Watershed Simulations." *Transactions of the ASABE* 50: 885–900. https://doi.org/10.13031/2013.23153.

Moriasi, D. N., M. W. Gitau, N. Pai, and P. Daggupati. 2015. "Hydrologic and Water Quality Models: Performance Measures and Evaluation Criteria." *Transactions of the ASABE* 58: 1763–1785. https://doi.org/10.13031/trans.58.10715.

Nash, J. E., and J. V. Sutcliffe. 1970. "River Flow Forecasting Through Conceptual Models Part I—A Discussion of Principles." *Journal of Hydrology* 10: 282–290. https://doi.org/10.1016/0022-1694(70)90255-6.

Neitsch, S. L., J. G. Arnold, J. R. Kiniry, and J. R. Williams. 2011. *Soil and Water Assessment Tool Theoretical Documentation Version 2009*. Texas Water Resources Institute.

O'Neill, B. C., C. Tebaldi, D. P. van Vuuren, et al. 2016. "The Scenario Model Intercomparison Project (ScenarioMIP) for CMIP6." *Geoscientific Model Development* 9: 3461–3482. https://doi.org/10.5194/gmd-9-3461-2016.

Özcan, Z., E. Kentel, and E. Alp. 2016. "Determination of Unit Nutrient Loads for Different Land Uses in Wet Periods Through Modelling and Optimization for a Semi-Arid Region." *Journal of Hydrology* 540: 40–49. https://doi.org/10.1016/j.jhydrol.2016.05.074.

Rathjens, H., K. Bieger, R. Srinivasan, I. Chaubey, and J. G. Arnold. 2016. "CMhyd User Manual: Documentation for Preparing Simulated Climate Change Data for Hydrologic Impact Studies." Accessed May 25, 2022. https://swat.tamu.edu/media/115265/bias_cor_man.pdf.

Riahi, K., D. P. van Vuuren, E. Kriegler, et al. 2017. "The Shared Socioeconomic Pathways and Their Energy, Land Use, and Greenhouse Gas Emissions Implications: An Overview." *Global Environmental Change* 42: 153–168. https://doi.org/10.1016/j.gloenvcha.2016.05.009.

Roberts, N. M., and H. W. Lean. 2008. "Scale-Selective Verification of Rainfall Accumulations From High-Resolution Forecasts of Convective Events." *Monthly Weather Review* 136: 78–97. https://doi.org/10.1175/2007MWR2123.1.

Schulzweida, U. 2021. *CDO User Guide Version 2.0.5*. Max Planck Institute for Meteorology.

Seker, M., and V. Gumus. 2022. "Projection of Temperature and Precipitation in the Mediterranean Region Through Multi-Model Ensemble From CMIP6." *Atmospheric Research* 280: 106440. https://doi.org/10.1016/j.atmosres.2022.106440.

Stouffer, R. J., V. Eyring, G. A. Meehl, et al. 2017. "CMIP5 Scientific Gaps and Recommendations for CMIP6." *Bulletin of the American Meteorological Society* 98: 95–105. https://doi.org/10.1175/BAMS-D-15-00013.1.

Sun, C., L. Zhu, Y. Liu, T. Wei, and Z. Guo. 2022. "CMIP6 Model Simulation of Concurrent Continental Warming Holes in Eurasia and North America Since 1990 and Their Relation to the Indo-Pacific SST Warming." *Global and Planetary Change* 213: 103824. https://doi.org/10.1016/j.gloplacha.2022.103824.

SYGM (General Directorate of Water Management). 2020. *Flood Management Plan of the Seyhan Basin*. General Directorate of Water Management.

Tokarska, K. B., M. B. Stolpe, S. Sippel, et al. 2020. "Past Warming Trend Constrains Future Warming in CMIP6 Models." *Science Advances* 6: eaaz9549. https://doi.org/10.1126/sciadv.aaz9549.

Tramblay, Y., A. Koutroulis, L. Samaniego, et al. 2020. "Challenges for Drought Assessment in the Mediterranean Region Under Future Climate Scenarios." *Earth-Science Reviews* 210: 103348. https://doi.org/10.1016/j.earscirev.2020.103348.

USGS (United States Geological Survey). 2014. "Shuttle Radar Topography Mission (SRTM): 1 Arc-Second Global Elevation Database." Accessed August 22, 2023. https://earthexplorer.usgs.gov/.

Usul, N. 2009. *Engineering Hydrology*. METU Press.

Wang, H.-M., J. Chen, C.-Y. Xu, J. Zhang, and H. Chen. 2020. "A Framework to Quantify the Uncertainty Contribution of GCMs Over Multiple Sources in Hydrological Impacts of Climate Change." *Earth's Future* 8: e2020EF001602. https://doi.org/10.1029/2020EF001602.

Yalcin, E. 2019. "Estimation of Irrigation Return Flow on Monthly Time Resolution Using SWAT Model Under Limited Data Availability." *Hydrological Sciences Journal* 64: 1588–1604. https://doi.org/10.1080/02626667.2019.1662025.

Yalcin, E. 2024. "A CMIP6 Multi-Model Ensemble-Based Analysis of Potential Climate Change Impacts on Irrigation Water Demand and Supply Using SWAT and CROPWAT Models: A Case Study of Akmese Dam, Turkey." *Theoretical and Applied Climatology* 155: 679–699. https://doi.org/10.1007/s00704-023-04657-0.

Zittis, G., M. Almazroui, P. Alpert, et al. 2022. "Climate Change and Weather Extremes in the Eastern Mediterranean and Middle East." *Reviews of Geophysics* 60: e2021RG000762. https://doi.org/10.1029/2021RG000762.

Supporting Information

Additional supporting information can be found online in the Supporting Information section. **Data S1:** jawr70084-sup-0001-Supinfo.docx.